Meteorol Atmos Phys 100, 195–206 (2008)
DOI 10.1007/s00703-008-0303-x
Printed in The Netherlands

Meteorology and Atmospheric Physics

[1] State Key Laboratory of Numerical Modeling for Atmospheric Sciences and Geophysical Fluid Dynamics, Institute of Atmospheric Physics, Chinese Academy of Sciences, Beijing, P.R. China
[2] Graduate University of Chinese Academy of Sciences, Beijing, P.R. China

The effects of diabatic heating on asymmetric instability and the Asian extreme climate events

L. Guo[1,2], **Y. Liu**[1]

With 8 Figures

Received 1 November 2007; Accepted 2 February 2008
Published online 14 August 2008

Summary

This paper analyzes the circulation during the extreme rainfall period in June 2003 over East China, and the effects of a tropical storm on the occurrence of the asymmetrical instability along the subtropics. It was found that ten days before the flooding in the Huaihe River reaches (115–120° E, 32–34° N) in East China, Typhoon (TC) Soudelor appeared over the western Pacific. Due to the strong latent heating released from the TC, the South Asia High (SAH) extended eastwards anomalously and formed an upper troposphere anticyclonic gyre (UTAG) over the western Pacific and a high potential vorticity (PV) downslided equatorwards to the east of the UTAG. When the deep high PV moved downwards to the easterlies, it was located in the south of the subtropical anticyclone over the western Pacific (SAWP) at a lower level. It moved westwards together with the SAWP, leading to the severe rainfall over East China.

An atmosphere circulation model is then used to investigate the physical link between the convection associated with the TC and the anomalies of the SAH, the high PV evolution as well as the variation of the SAWP. It is shown that the introducing of a typhoon-like heating over the tropics in the model results in the occurrence of pronounced asymmetrically instability (AI). In the upper troposphere, the anticyclonic flow as well as the development of the equatorward downsliding high PV are predominantly forced by the heating. The response is sensitive to the intensity, domain and location of the heating prescribed within the zonal wind. The larger size and the stronger intensity the heating is, the more prominent the anticyclone and the downsliding high PV are.

It is also demonstrated that there exists a critical heating rate of the subtropical forcing for the occurrence of AI. Under the June zonal symmetric flow the critical heating rate is about 3 K day^{-1}. Moreover, a heating in tropics or subtropics tends to generate stronger instabilities than in mid-latitude westerlies. In mid-latitude a forcing can generate downstream propagating Rossby wave along the westerlies easier. Finally, the results from an experiment with the inclusion of "realistic" synthetic heating over the western Pacific are in consistence with the observational behavior.

Correspondence: Yimin Liu, LASG, Institute of Atmospheric Physics, Chinese Academy of Sciences, Beijing 100029, P.R. China (E-mail: lym@lasg.iap.ac.cn)

1. Introduction

In summer, the dominant circulation feature in the upper troposphere is the pronounced upper level anticyclone over South Asia, namely South Asia High (SAH), and the tropic upper tropospheric trough. In the middle troposphere over East Asia, the dominant feature is the variation of Subtropical Anticyclone over the Western Pacific (SAWP). Baroclinic instability is one of the important mechanisms which influence mid-latitude atmospheric circulation (Holton 2004). Diabatic heating released by precipitation along East Asia

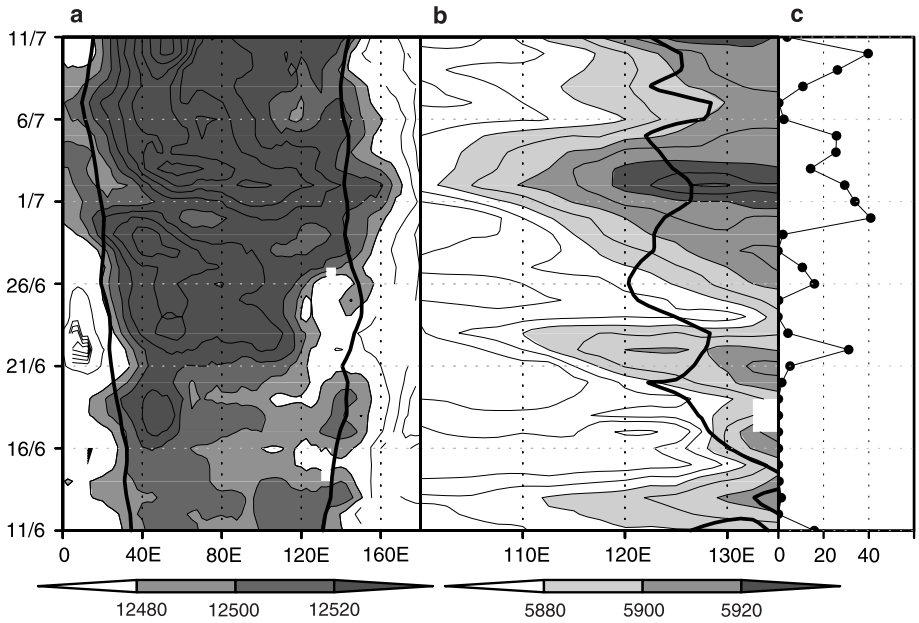

Fig. 1. (**a**) Evolution of 200 hPa geopotential high (gpm) along the ridge of South Asia High. Greater than 12480 gpm is shaded. Interval is 20 gpm. Thick solid contour is its climate mean of 12480 gpm. (**b**) Evolution of 500 hPa geopotential high (gpm) along the ridge of SAWP. Greater than 5880 gpm are shaded. Interval is 20 gpm. Thick solid contour is its climate mean of 5880 gpm. (**c**) Precipitation rate (mm/day) time series for the period June 11–July 11, 2003 in Huaihe River reaches (115–120° E, 32–34° N)

coast can cause latitudinally asymmetric disturbance, and can cause baroclinic instability (Hoskins and Karoly 1981). On the other hand, the location and intensity of the precipitation over East China has a close relationship with the SAWP (Wu et al. 2002). Therefore it is necessary to investigate the variation of the SAH and SAWP and their interaction with the heavy rainfall over Eastern Asia.

The rainfall extreme was an important feature in 2003 of the summer climate over China (Levinson and Waple 2004). Huaihe River reaches (115–120° E, 32–34° N) experienced above-normal precipitation and flooding. Severe heavy rainfall in the Huaihe River reaches started from June 21 to July 11, lasting 21 days. During this period SAH at 200 hPa extended further eastwards comparing with its climatic mean and correspondingly, the SAWP at 500 hPa shifted westwards (Liu et al. 2006; Yao et al. 2007). Thus the Huaihe River reaches was controlled by the upper layer divergence of the eastern SAH and the lower layer southwesterlies of the western SAWP which are favorable to the occurrence of severe rainfall (Dao and Chu 1964). Yao et al. (2007) also found that there was a thick cyclonic eddy in the easterlies in the mid-high altitudes moving westwards along with the moving of SAWP from June 19 to June 24. When the cyclonic eddy was almost in the same longitude with a westerly trough in middle latitude, the SAWP retreated eastwards and the heavy rainfall over the Huaihe River reaches intermitted for two days. The rainfall continued when the SAH extended eastwards as well as the SAWP (Fig. 1) and another cyclonic eddy moved westwards (figure not shown). Moreover, the simultaneity of the severe rainfall over eastern China and the cyclonic eddy moving westwards happened a few times in summer according to the investigation started from 2003 (Liu[1]). Why did the SAH extend eastwards and where did the cyclonic eddy, which could be presented by high potential vorticity (PV), come from?

Hsu and Plumb (2000) suggested a mechanism for the variability of the SAH based on their idealized shallow water equation experiments. They showed that with sufficiently large asymmetric forcing, the forced anticyclone becomes unstable and periodically sheds eddies westwards. Liu et al. (2007) demonstrated that such an oscillation owes its existence to the diabatic heating

[1] Liu Huanzhu, private communication.

over the TP by using an adiabatic spectral primitive equation model. Then, what is the response of the SAH when there is a diabatic heating source in an AGCM which includes the interaction of heating and circulation? On the other hand, there is a high PV reservoir in high altitudes and latitudes (Hoskins et al. 1985). Does the cyclonic eddy with high PV in the easterlies come from the PV reservoir? If it does, why does the high PV eddy split from the high PV belts?

The aim of this research is to demonstrate that the diabatic heating associated with the severe weather events along the East Asia does produce the asymmetric instability (AI) and further influence the subtropical circulation and summer climate in China in 2003 by using numerical experiments. There were several peaks of the heavy rainfall in this summer (Fig. 1c) and the first process during 21st–23rd indicating the start of severe raining or Meiyu of the Huaihe River reaches and will be investigated in this study. The layout of the paper is as follows. In Sect. 2, we introduce the model and data used. Although some analyses have been carried out on the synoptic-scale features associated with the 2003 Huaihe River reaches flooding (see references in the beginning of this section), it is useful to describe briefly the evolution of some variables from PV $-\theta$ view to provide the background to evaluate the model results. Such an overview of the circulation variation is offered in Sect. 3. In Sect. 4, we discuss the model simulations. It includes the diagnoses of instabilities in several idealized numerical experiments, and is followed by the simulation of the influence of the diabatic heating in East Asia in 2003 summer in Sect. 5. Section 6 provides concluding remarks.

2. Model and data

The model we used is called SAMIL (Spectral Atmospheric Model of IAP LASG), developed at the Institute of Atmospheric Physics/State Key Laboratory of Numerical Modeling for Atmospheric Sciences and Geophysical Fluid Dynamics (LASG/IAP) based on the LASG/R15L9 (Wu et al. 1996). It is a rhomboidally truncated spectral model. Its horizontal resolution is approximately a 2.8125° longitude $\times$ 1.67° latitude transformed grid. There are 26 levels in $\sigma - P$ hybrid coordinate in the vertical. The standard atmosphere concept was introduced to the model by subtracting a standard atmospheric profile of temperature and pressure to reduce errors. Semi-implicit time integration is used. Physical parameterizations include the updated radiation parametric scheme developed by Edwards and Slingo (1996), diagnostic cloud parameterization, convection adjustment parameterization developed by Tiedtke (1989), and vertical and horizontal diffusion parameterization. The nonlocal Boundary Layer parameterization (Palmer et al. 1986) is adopted. SAMIL also considers orography and gravity wave drag in the physical process.

The daily rainfall data are the Global Precipitation Climatology Project (GPCP) (Huffman et al. 2001) during June 2003. National Center for Environmental Prediction (NCEP) reanalysis daily mean data (Kalnay et al. 1996), including temperature and horizontal wind et al. are used. In subtropical area, the 345 K isentropic surface is close to the altitude of 200 hPa isobar surface. To show how PV varies at upper troposphere, PV at the 345 K isentropic surface is also constructed from the above data.

3. Observational overview

In association with the first severe rainfall over the Huaihe River reaches from 21st to 23rd June 2003 (Fig. 1c), the variation of the corresponding flow could be divided into two stages. The first one was from 15th to 18th. Figure 2 shows the PV and wind at 345 K surface as well as the principal parts of the SAH and SAWP from 15th to 24th June. Although the eastern part of the SAH represented by the contour of 12480 gpm located along almost the same location as its climatology, i.e. 120° E on 15th June, the anticyclonic flow associated with low PV extended northeastwards over the northwest Pacific. The anticyclonic flow and the High (the dashed contours) became stronger and even formed an upper troposphere anticyclonic gyre (UTAG) over the western Pacific in the subsequent days. From June 16th to 19th, the east edge of the UTAG extended from 140° E to 160° E. To the east of the UTAG, the northerlies led the high PV southwards to the easterlies along the isentropic surface by day 17. The high PV was broken away from the trough in high latitudes and was advected west-

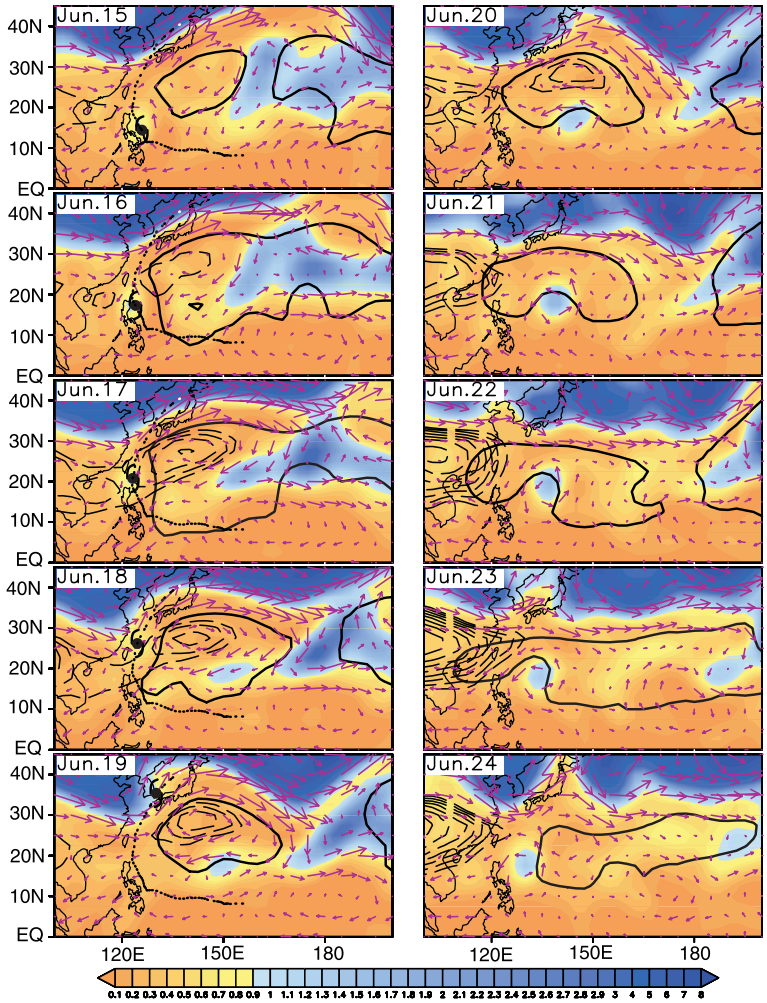

Fig. 2. Distributions of wind ($m\,s^{-1}$) and PV (shaded, unit: PVU) at 345 K isentropic surface, geopotential high greater than 12480 gpm (dashed contour, interval is 10 gpm) at 200 hPa and geopotential high of 5880 gpm (thick solid contour) at 500 hPa over East Asia. Dotted contour is TC track for June 11–19. The typhoon symbol is averaged TC eye during that day

wards to the south of the UTAG, and then it was isolated and became a cyclonic eddy by June 18th. The western part of the SAWP was almost located in the west of 130° E stably during this stage (Fig. 1b) and showed a barotropic structure over the western Pacific with the UTAG aloft (Fig. 2, day 16–18).

It is interesting to notice that Typhoon (TC) Soudelor was generated on 11th June and located in the east of Philippine on June 15th (Fig. 2). By this day Soudelor has become a strong tropical storm and brought heavy precipitation over the western Pacific (http://www.typhoon.gov.cn/). There was a strong condensation heating associated with the typhoon. From June 13rd, the maximum heating rate was about 15 $K\,day^{-1}$ located between 300 and 400 hPa (figure not show). This intensity sustained and enhanced for the following 4 days and was greater than 15 $K\,day^{-1}$ again by June 19th. The strong condensation heating release in the TC has impacts on the large-scale circulation variability over the tropical western Pacific (Harr and Elsberry 1995; Soble and Camargo 2005; Ren et al. 2007). The heating leads to high pressure and divergence aloft and may contribute to the variation of the SAH and SAWP shown in Figs. 1 and 2. We suggest that it is the response of the SAH to the heating so that the UTAG was formed and the northerlies of the east portion of the UTAG inducted the high PV moving southwards from higher latitudes. In the next section we will verify the above hypotheses using numerical experiments.

The main feature of the flow during the second stage from 19th to 24th was the westward shifting of the high PV eddy moving together with the SAWP extended westwards in the easterlies. We will discuss this later in the modeling section. The high PV-cyclonic eddy was only in the middle and high troposphere and could not be detected at 320 K surface where the pressure is

about 600 hPa along 20° N (figure not show). On 21st when the SAWP located to the west of its climatic place (Fig. 1b), the southwesterlies in the west of the SAWP transported moisture to the Huaihe River reaches and the heavy rainfall started (Fig. 1c). By June 24th, this high PV was almost near the same longitude with a westerly trough in middle latitude, positive vorticity increased and the SAWP weakened to the west of 130° E (Yao et al. 2007). This is due to the instability mechanism, i.e. when two PV anomaly patterns are less than a quarter wavelength out of phase with each other, mixed instability developed (Hoskins et al. 1985).

The above results suggest that the convective heating associated with the TC over the western Pacific generated instability and might contribute to the variation of the UTAG and then induced the high PV splitting from high latitudes. The high PV moved southwards and surrounded the SAWP to its east and south, so the SAWP became unstable and extended westwards. Such reasoning will be tested by using the SAMIL in the next sections.

4. Idealized condensation-heating experiments

4.1 Experiment set-up

In this study, sea surface temperature and sea ice are June zonal averaged climate mean ranging from 1978–88 which is developed for the Atmospheric Model Intercomparison Project (AMIP). The initial fields are June zonal mean climate averaged NCEP reanalysis data. All the experiments are aqua-planet ones, and are perpetual runs, in which the solar zenith angle is fixed on 15th June.

In our experiments, we put a vertically varying latent heating source in the zonal symmetric flow, at day 6 after the spin-up of the model atmosphere's adjustment. The vertical distribution of latent heating is added in troposphere ranged from 750 hPa to 150 hPa. The maximum heating rate is located at 345 hPa following the vertical structure of Q1 (Yanai et al. 1973) of TC center. The heating rate decreases gradually to 0 at 150 hPa above and 750 hPa below. In order to investigate the sensitivity of the response, we change the intensity, domain and position of latent heating source and divide the experiments into three group, as shown in Table 1.

Table 1. Experiments of different heating forcing. Exps. 1–3 are intensity experiments, Exp. 4 is latitudinal domain experiment, Exps. 5–7 are position experiments

Exp.	Intensity (K)	Position	Range (°)
1	10	140–150° E, 5–25° N	10 × 20
2	6	140–150° E, 5–25° N	10 × 20
3	4	140–150° E, 5–25° N	10 × 20
4	6	120–150° E, 5–25° N	30 × 20
5	4	140–150° E, 5–15° N	10 × 20
6	4	140–150° E, 15–35° N	10 × 20
7	4	140–150° E, 25–45° N	10 × 20

4.2 Intensity experiments

To mimic the strong condensation heating release of the TC over the western Pacific, a deep condensation heating is imposed, i.e. in the region from 140 to 150° E and between 5 and 25° N, with a maximum heating of 10 K day^{-1} as depicted by the box in Fig. 3a (Exp. 1). The circulation derived from two other experiments with the maximum heating rate of 6 K day^{-1} and 4 K day^{-1}, respectively are also presented to reveal the sensitivity to the atmospheric response to forcing intensity (Fig. 3b and c; Exps. 2 and 3). The similarity among Exps. 1–3 is that the zonally symmetrical circulation is destroyed when the forcing is added. Take the 4 K case for example. By day 1, an anticyclonic flow appears at 345 K isentropic surface above the heating source (Fig. 3c). By day 5, the flow has become a closed anticyclonic gyre, UTAG, shown by the contour line of the geopotential field at 200 hPa. This response can be explained by the PV – θ view proposed by Hoskins (1991). Therefore, as a first approximation, the circulation at day 1 as presented in Fig. 3 can be interpreted as the adaptation of atmospheric circulation to the diabatic heating (Wu and Liu 2000). The upper level anticyclone moves eastwards from day 8 due to the strong advection in the westerlies in mid-latitude. Comparison of Fig. 3a, b and c shows that the larger the heating is, the stronger the upper level anticyclonic vorticity is. By day 10, the UTAG extends eastwards further in Fig. 3a than in Fig. 3b and c due to stronger advection. The eastern boundary represented by the 12180 hPa contour reaches to 170° W, 180° E, and 170° E for the 10 K (Exp. 1), 6 K (Exp. 2) and 4 K (Exp. 3) experiments, respectively. A higher PV slides

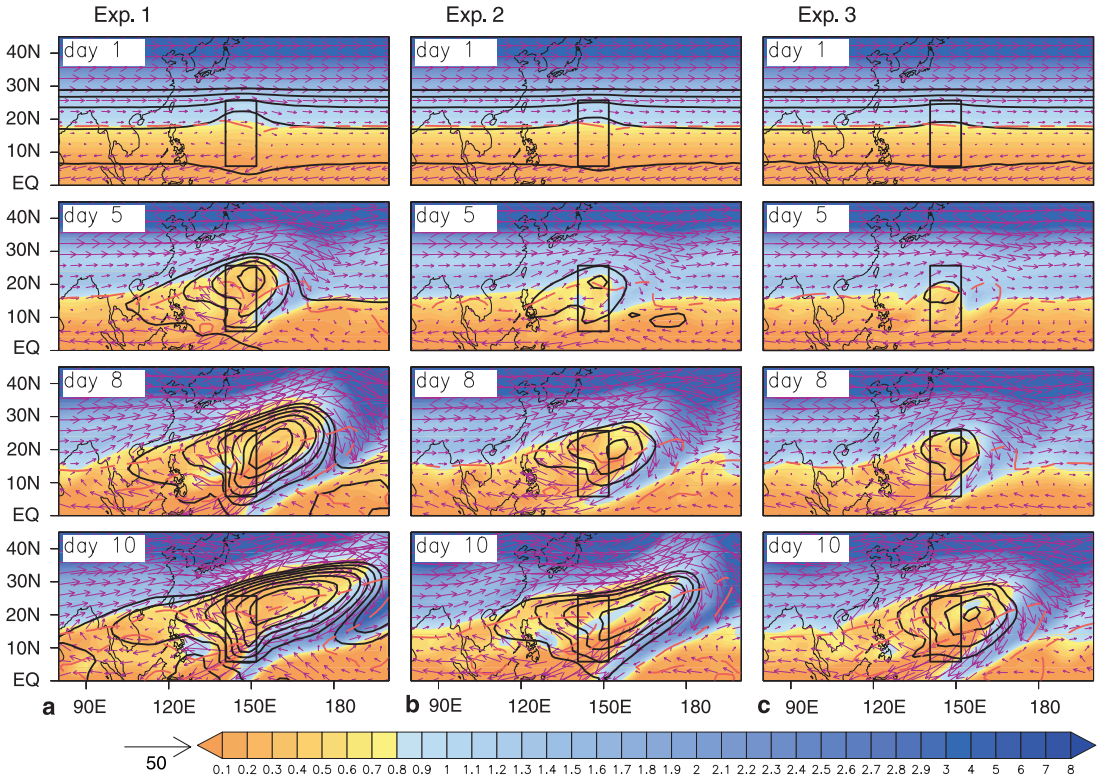

Fig. 3. Distributions of wind ($m\,s^{-1}$), and PV (shaded, unit: PVU) at 345 K isentropic surface and geopotential high greater than 12180 gpm (contour) at 200 hPa for intensity experiments, with the interval of 10 gpm. Red dash contour is $u = 0$ at 300 hPa. Rectangle is heating area with a maximum heating rate of (**a**) Exp. 1 of $10\,K\,day^{-1}$; (**b**) Exp. 2 of $6\,K\,day^{-1}$; and (**c**) Exp. 3 of $4\,K\,day^{-1}$, respectively

southwards from mid-latitude guided by the northerlies at the eastern portion of anticyclone from day 5, and arrives in the easterlies at day 6 (figure not shown). This is in agreement with the timing of the high PV vortex arriving to the tropics on 17 June, 6 days after the TC generated on 11 June in the observation. The high moves along the intensified easterlies and starts to shift westwards by day 8.

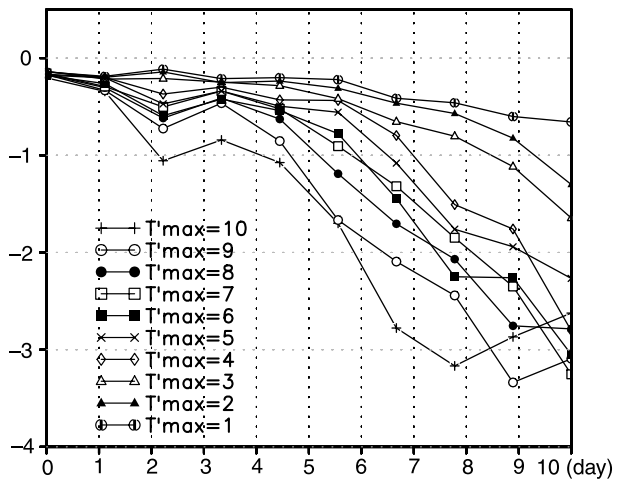

Fig. 4. Area averaged southward PV flux ($PVU \cdot m\,s^{-1}$) over 0–25° N, 0–360° E at the 345 K isentropic surface from the ten intensity experiments

Ten experiments with different heating intensity ranged from 1 to 10 K were run to investigate the differences of the asymmetric instability. Figure 4 shows the evolution of area mean southward PV flux at 345 K isentropic surface calculated from the 10 experiments. The northerlies appears earlier and are stronger in the stronger heating experiments, so the southward PV flux is stronger. The flux increases with the increasing of the heating strength especially during the first 8 days, presenting the linear response of model atmosphere to the forcing within a short period.

From these series of the experiments, we find that the critical heating intensity of separating stable and unstable PV cases lies at $3\,K\,day^{-1}$. We can infer from the results that, for a stable non-axisymmetric circulation to exist under the June uniform flow, the magnitude of the maximum heating cannot be much larger than $3\,K\,day^{-1}$.

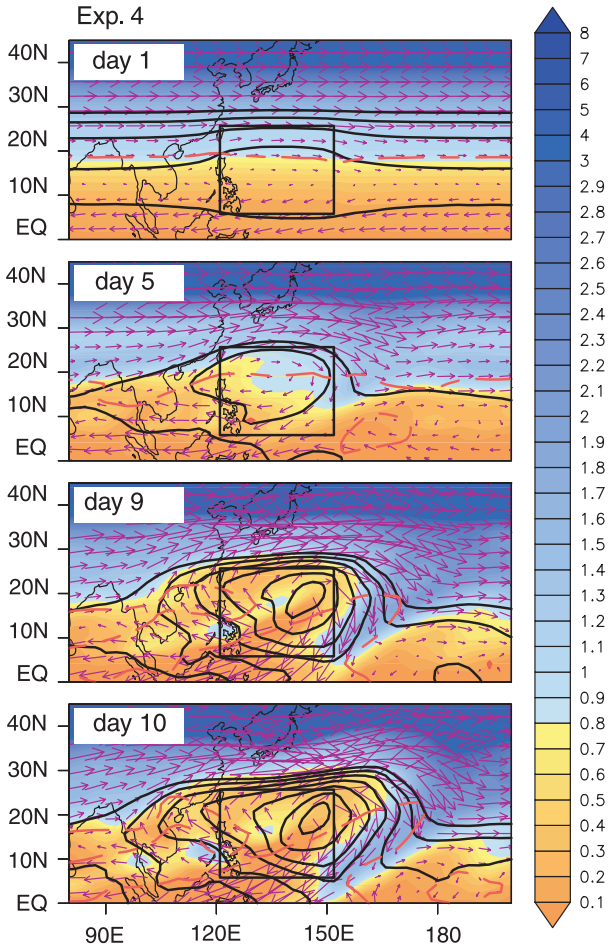

Fig. 5. The same as Fig. 3b, but for Exp. 4 of 6 K day^{-1}

If the heating is strong enough, i.e. larger than 3 K day^{-1}, the PV distribution becomes non-zonally oriented, and the induced return flow is strong enough to prevent the anticyclonic vorticity from being advected downstream by the westerly flow.

4.3 Domain experiments

Altering the heating domain results in a different response. Figures 3b and 5 shows the circulation pattern from two experiments which have the same maximum heating rate 6 K day^{-1} but different latitudinal domain which the latter extended 20 degrees wider compared to the former. The strength of the northerlies to the east of the UTAG is almost the same within the first 5 days in Figs. 3b and 5. It means that the occurrence of the northerlies is mainly related to the strength of forcing before the advection occurs and the convection adjustment appears. We will discuss the adjustment later. The difference between these two experiments is that the UTAG forced by the wider heating (Fig. 5) is stronger than that by the normal one (Fig. 3b) especially after day 5. Accordingly, northerlies anomaly is much stronger in Fig. 5 after day 5. This difference can be explained by the relationship between vorticity variation and heating from the complete vorticity equation developed by Wu et al. (1999) and Liu et al. (2001):

$$\frac{\partial \zeta}{\partial t} \propto \frac{f+\zeta}{\theta_z}\frac{\partial Q}{\partial z} \tag{1}$$

where ζ is the vertical component of the relative vorticity, f is the Coriolis parameter, θ is the potential temperature, $\theta_z = \frac{\partial \theta}{\partial z}$. Q is the diabatic heating. When air particles go through a wider domain heating source (Fig. 5), they get more time to be heated so the vorticity response is stronger at the upper troposphere. This case is similar to the quadruple heating pattern (Wu and Liu 2003; Liu et al. 2004) over land in subtropics which shows that the SAH over the huge Euro-Asia continent is much stronger than the anticyclone over the north-America continent (the Tibetan Plateau contributes to the formation of the SAH as well).

Another difference between the two experiments is that the UTAG is anchored over the heating source before day 9 in Fig. 5 reflecting the thermal adaptation of the atmosphere to the heating (Liu et al. 2004); while the gyre extends northeastwards to the heating in Fig. 3b. This is due to the different locations of latent heating release as the result of convection adjustment of the model atmosphere after the prescribed heating. An additional latent heating is located on the east of the prescribed heating source in the wider domain experiment (figure not shown). Thus the northerly anomaly exits over heating area at upper level with the anticyclone locates on its west, which follows the Sverdrup balance suggested by Liu et al. (1999, 2001) and Rodwell and Hoskins (2001).

4.4 Position experiments

The response to a heating forcing may vary by the prescribed heating in different latitudes. Figure 6 shows the results from another series of experiments integrated with a heating which have the same intensity but locating at different latitudes (Exps. 5–7). The domain of the heating in Exp. 5 (Fig. 6a) is smaller so the heating is in the east-

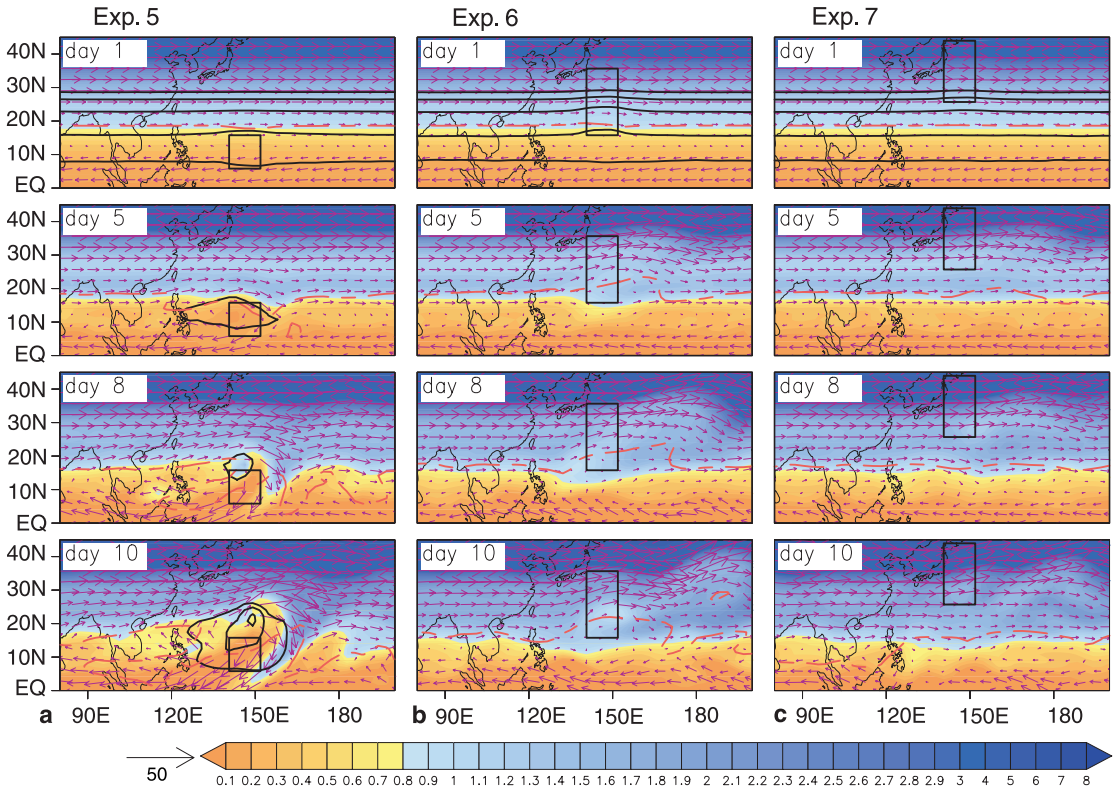

Fig. 6. The same as Fig. 3, but for (**a**) Exp. 5, (**b**) Exp. 6, and (**c**) Exp. 7, respectively

erlies in this experiment. The upper level circulation exhibits pronounced differences in the three experiments. The anticyclonic flow can be found only in Fig. 6a and b and the southwards shifting high PV only appears in Exp. 5 (Fig. 6a). Moreover, the response in Exp. 5 (Fig. 6a) shows only a small dispersion due to the perturbation in tropics (Hoskins and Jin 1991). On the other hand, although the downward Rossby wave stimulated by the heating exists in all the three experiment after day 8, Rossby wave is not yielded in Exp. 5 at the beginning of the integration until the perturbation is transfered to the westerlies due to the divergence from day 8. Comparing Figs. 6 and 3, we can conclude that a forcing in tropics (easterlies) and subtropics can generate asymmetric instabilities more easily than in mid-high latitudes (westerlies) due to stronger advection dispersion in the later case. When the heating locates in westerlies it has weaker impact on the subtropical flow.

4.5 Evolution of the SAWP

As discussed in Sect. 3, the westward shifting high PV eddy moved in the easterlies together with the SAWP westward extension after TC weakening during the second stage (June 19th–24th) of the first severe rainfall over Huaihe River reaches. The southwesterlies to the west of the SAWP transported moisture to the Huaihe River reaches and the heavy rainfall started. In this section, we shut down the prescribed latent heating forcing after the end of the 10th model day based on Exp. 1 and investigate the circulation variation in the subsequent few days.

At 345 K isentropic surface, the UTAG sustains without the latent heating forcing. The high PV still slides southwards from mid-latitude and move westwards continually (figure not shown, refer to the bottom panel of Fig. 3a). Figure 7 shows the evolution of the SAWP and the vertical velocity at 500 hPa starting from the last day with the heating forcing (day 10). At day 10 a closed high (SAWP) is located over the western Pacific and barotropic structure is found which are in consistence with the observation at 19th June (Fig. 2). By day 11, precipitation (denoted by the ascent in Fig. 7) develops along with the southerlies to the west of the SAWP. From day 11 to day 13, the SAWP extends fifteen longi-

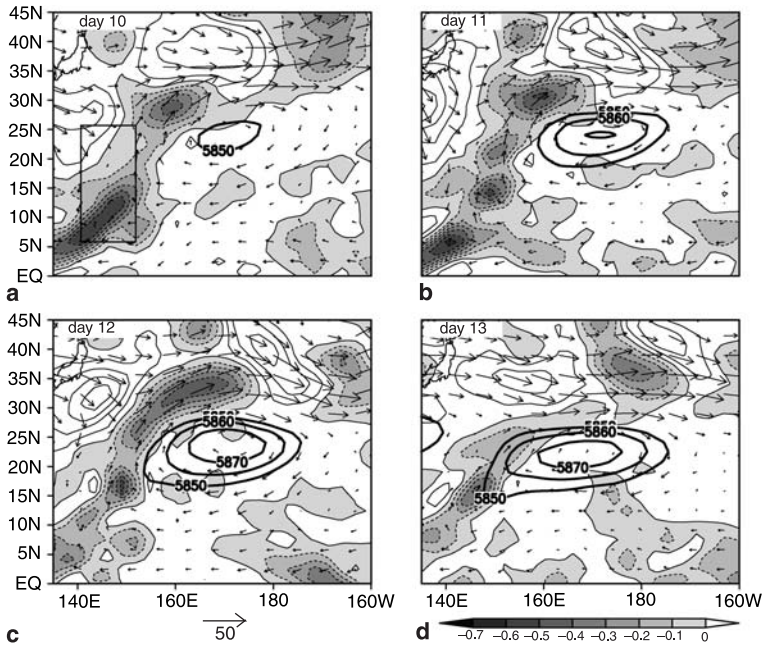

Fig. 7. Distributions of 850 hPa wind ($m\,s^{-1}$), ω (Pa/s) (thin contour) and geopotential high (gpm) greater than 5850 gpm (thick solid contour) at 500 hPa for the integration without heating continued from day 10 of Exp. 1. $\omega \leq 0$ is shaded

tudes westwards being in consistence with observation from 19th to 21st (Fig. 2). The westward extension can be regarded as the role of the advection by the anticyclone of high PV around from the east and low PV to the west (Hsu and Plume 2000; Liu et al. 2007). Therefore the effect of the TC can at least partly reveal the mechanism of the variation of the SAH and SAWP as well as the heavy rainfall over Huaihe River reaches in 2003.

5. Experiments with the synthetic heating imitating 2003 summer

Based on the study in above sections, we investigate further the impacts of the heating following the pattern in 2003 summer. Three experiments are designed as shown in Table 2 to simulate the first rainfall process. In Exp. 8, a very strong latent heating with the intensity as strong as TC is prescribed in low latitudes. The heating region imitates the area of the heavy TC rainfall of more than $10\,mm\,day^{-1}$ from GPCP averaged over June 16th–20th. In Exp. 9 a weak heating source locates in 20–30° N to simulate the local weak convection; and in Exp. 10, both the heating sources are set in the same longitudes to simulate the first course of severe heavy rainfall in the Huaihe River reaches in 2003.

The UTAG appears by the 1st day under the strong latent heating forcing in Exp. 8 (Fig. 8a).

Table 2. Experiments of observational pattern simulations

Exp.	Intensity (K)	Position	Range (°)
8	15	120–130° E, 5–15° N	10×10
9	6	120–130° E, 20–30° N	10×10
10	15	120–130° E, 5–15° N	10×10
	6	120–130° E, 20–30° N	10×10

The anticyclonic gyre by day 5 shows only small dispersion again but is much stronger than that with the weaker heating by day 10 in Exp. 5 (Fig. 6a). High PV starts to shift by day 5 and moves further southwards than the weaker heating case. The intensity and range of UTAG keep extending. By day 8 the north portion of the anticyclone reaches 30° N in the westerlies so the UTAG starts to move eastwards. On the other hand the high PV slides equatorward along the strong northerlies, and then moves westwards in the easterly at low latitudes. It produces strong cyclonic disturbance at lower levels as well.

In Exp. 9 only weak mid-latitude disturbance is produced and there is no closed anticyclone and no high PV being conducted to the lower latitudes (Fig. 8b). However, such mid-latitude disturbance can propagate downstream in the westerlies as for the existence of Rossby wave packet. By day 5, 8 and 10, this disturbance arrives at 160, 170, and 180° E, respectively.

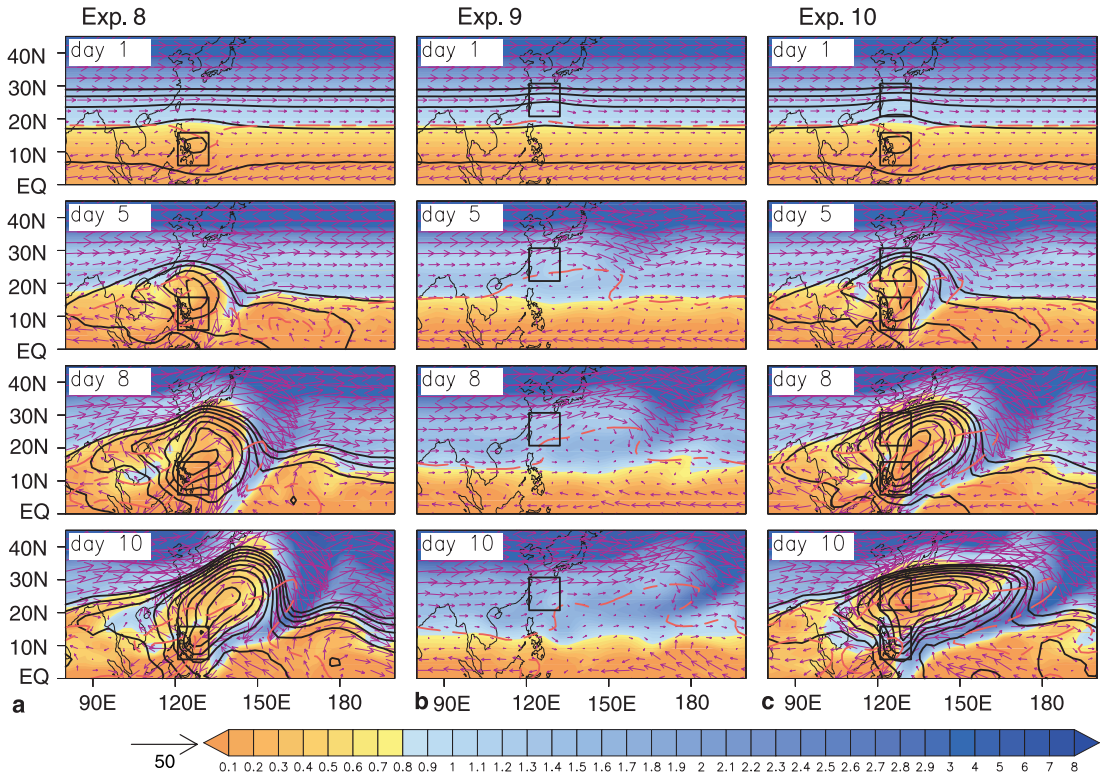

Fig. 8. The same as Fig. 3, but for Exp. 8, Exp. 9, and Exp. 10, respectively

With both the above heating, in Exp. 10 (Fig. 8c), the result is similar to that in Exp. 8 in the first five days (Fig. 8a). By day 8, the intensity of the UTAG in Exp. 10 is similar to the UTAG in Exp. 8, but the former range extends more eastwards. The maximum northerlies near 170° E, which is similar to the location of the propagation of maximum amplitude in Exp. 9. The high sliding PV extends more eastwards too. By day 10, the eastern edge of UTAG reached to 180° E in Exp. 10.

The results from the above three experiments again show that the anomaly of the upper level anticyclone gyre and the southward downsliding high PV are closely related to the intensity of the tropical forcing source. On the other hand, the location of the forced UTAG is affected by the forcing in westerlies shown in Exp. 9 since such heating helps the unstable energy propagating downstream further. Without it, the northerly anomaly forced by the tropic forcing (Exp. 8, Fig. 8a) appears at lower latitudes at the beginning of the integration so the high PV shifts southwards later than that in Exp. 10 (Fig. 8c).

Although the heavy rainfall of more than 30 mm day^{-1} of the TC Soudelor maintained 9 days from June 11th to 19th (http://precip.gsfc.nasa.gov/), the location was not at the same place and its intensity also varied. In contract, all results in this paper are from idealized numerical experiments with fixed stationary forcing. This may be the reason of that the high PV is split and becomes a vortex in the observation (Fig. 2), but the high PV is linked with that in high latitudes in the numerical experiments. However, there are considerable agreements between model behaviors and the observations (Fig. 2), such as the western extention of the SAWP and its barotropic structure (Fig. 7), the UTAG, and the equatorward moving high PV 5 days after the heating is turned on (Fig. 8c). As shown in Fig. 2 on June 18, the eastern portion of the UTAG can reach 180° E, 50° E to the TC heating, which is well simulated in Exp. 10 (Fig. 8c).

One thing should be noted that we used the June zonal mean of wind as the initial flow which possesses too-strong westerly wind shear in the

subtropics. Therefore the results from Exp. 6 and Exp. 9 do not necessarily mean that a heating cannot yield the asymmetric PV instability when it is located at the range of 15–35° N. This is because the climatological interface of the westerlies and the easterlies is along 23° N at 200 hPa and 20° N at 500 hPa over the western Pacific in June, and the westerly over there is much weaker than its zonal mean case. Therefore we can expect much stronger asymmetric PV instability being generated if the real environment was employed in Exps. 6 and 9.

6. Concluding remarks

Based on the diagnosis and modeling of the Asian summer circulation during the severe heavy rainfall in the Huaihe River reaches in 2003, we investigate the impacts of diabatic heating on the AI and the corresponding development of the Asian summer circulation. It is confirmed that when SAH extends eastwards and a UTAG is generated over the western Pacific, the SAWP extends westwards and there was a cyclonic eddy within the easterlies over the western Pacific during the severe heavy rainfall in the Huaihe River reaches. Further, it is found that the eddy originates from the southwards downsliding high PV which was induced by the northerly on the east portion of the UTAG. The eddy broke off from the high PV reservoir in higher latitudes and moved westwards along easterlies. Very importantly, we notice that TC Soudelor over the western Pacific was observed ten days before the severe rainfall over East China. The condensation heating associated with the TC generated pronounced AI and had significant impacts on the atmospheric circulation.

The results from the numerical experiments document that strong tropical heating can result in an UTAG as well as the equatorward downsliding high PV to the east of the UTAG. In the stronger heating experiments the anomalous anticyclone is more remarkable. So are the northerly to its east and the southward PV flux. Although the model atmosphere presents a linear respond to the forcing intensity within the early days of the integration, the PV development becomes unstable when the heating rate exceeds a critical value of 3 K day^{-1} under the June zonal symmetric flow.

The response is also sensitive to the domain of the heating while the northerly to the east of the anticyclonic gyre is almost same at the beginning of the integration between the two domain experiments. The anticyclone is stronger in the larger domain one. The location of the anticyclone also varies in different heating domain experiments due to the convection adjustment process in the model, which reflects the reaction of the circulation to the prescribed forcing.

Location of the heating in different zonal wind also plays important roles in the occurrence of AI. A forcing in tropics (easterlies) and subtropics can generate asymmetric instabilities easier than that in mid-high latitudes (westerlies). The heating located in westerlies has littler impacts on the subtropical flow, but can generate downstream energy propagation due to the larger advection. The results from the experiment with a 'realistic' synthetic heating over the western Pacific are consistent with the observational behavior.

The implication from this study is that the real atmosphere may experience accelerated seasonal variation by an extreme weather event, such as a strong tropic storm in the western Pacific in 2003. Usually summer monsoon rainband in China occurs in South China in early June. In middle June this monsoon rainband reaches the Yangzhi River and is named as Meiyu. By the end of June, the forefront of the East Asian monsoon jumps to the southern border of North China, and mid-summer starts over the entire Asia (Tao and Chen 1981). In 2003, the rainfall stayed in South China until 21st June when Huaihe River Reached started suffering the severe rainfall. So the TC helped the rain to occur more suddenly over this area in this year. Since the relationship between the TC and large-scale circulation is complicated, the TC could also influence the large scale circulation through momentum and water vapor redistribution (Sobel and Camarago 2005).

Although this is a case study, the high PV eddy appears quite frequently during the heavy rainfall events, as discussed in the Introduction Section. Thus the results can help the understanding of the summer subtropical circulation and the associated extreme climate events over Asian.

Acknowledgements

The authors would like to thank Prof. Guoxiong Wu and Prof. Brian Hoskins for many constructive suggestions, and reviewers for helpful comments. This research was supported by the State Key Basic Research 2004CB418300 and 2006CB403607, and NSFC under grant no. 40575028, 40221503 and 40523001.

References

Dao SY, Chu FK (1964) The 100-mb flow patterns in southern Asia in summer and its relation to the advance and retreat of the west-oacioic subtropical anticyclone over the far east. Acta Meteorologica Sinica 4: 385–95 (in Chinese)

Edwards JM, Slingo A (1996) A studies with a fexible new radiation code. I: Choosing a configuration for a large-scale model. Q J Roy Meteor Soc 122: 689–720

Harr PA, Elsberry RL (1995) Large-scale circulation variability over the tropical western north Pacific. Part I: Spatial patterns and tropical cyclone characteristics. Mon Wea Rev 123: 1225–46

Holton JR (2004) An introduction to dynamic meteorology. Elsevier, Seattle, 535 pp

Hoskins BJ (1991) Towards a PV – θ view of the general circulation. Tellus 43AB: 27–35

Hoskins BJ, Jin FF (1991) The initial value problem for tropical pertubations to a baroclinic atmosphere. Q J Roy Meteor Soc 117: 299–317

Hoskins BJ, Karoly DJ (1981) The steady linear response of a spherical atmosphere to thermal and orographic forcing. J Atmos Sci 38: 1179–96

Hoskins BJ, Mcintyre ME, Robertson AW (1985) On the use and significance of isentropic potential vorticity maps. Q J Roy Meteor Soc 111: 877–946

Hsu CJ, Plumb RA (2000) Nonaxisymmetric thermally driven circulations and upper-tropospheric monsoon dynamics. J Atmos Sci 57: 1255–76

Huffman GJ, Adler RF, Morrissey MM, Bolvin DT, Curtis S, Joyce R, McGavock B, Susskind J (2001) Global precipitation at one-degree daily resolution from multi-satellite observations. J Hydrometeorol 2: 36–50

Kalnay E, Kanamitsu M, Kistler R, Collins W, Deaven D, Gandin L, Iredell M, Saha S, White G, Woollen J, Zhu Y, Leetmaa A, Reynolds B, Chelliah M, Ebisuzaki W, Higgins W, Janowiak J, Mo KC, Ropelewski C, Wang J, Jenne R, Joseph D (1996) The NCEP/NCAR 40-year reanalysis project. B Am Meteor Soc 77: 437–71

Levinson DH, Waple AM (2004) State of the Climate in 2003. B Am Meteor Soc 85: s1–72

Liu HZ, Zhao SR, Zhao CG, Lu ZS (2006) Weather abnormal and evolutions of western Pacific subtropical high and south Asian high in summer of 2003. Plateau Meteorol 25: 169–78 (in Chinese)

Liu YM, Hoskins BJ, Blackburn M (2007) Impacts of the Tibetan topography and thermal forcing over Asia in summer. J Meteor Soc Japan 85B: 1–19

Liu YM, Wu GX, Liu H, Liu P (1999) The effect of spatially non-uniform heating on the formation and variation of subtropical high. Part III: Condensation heating and south Asia high and western Pacific subtropical high. Acta Meteor Sinica 57: 525–38 (in Chinese)

Liu YM, Wu GX, Liu H, Liu P (2001) Condensation heating of the Asian summer monsoon and the subtropical anticyclone in the Eastern Hemisphere. Clim Dynam 17: 327–38

Liu YM, Wu GX, Ren RC (2004) Relationship between the subtropical anticyclone and diabatic heating. J Climate 17: 682–98

Palmer TN, Shutts G, Swinbank R (1986) Alleviation of a systematic westerly bias in general circulation and numerical weat her prediction models through an orographic gravity wave drag parameterization. Q J Roy Meteor Soc 112: 1001–39

Ren SL, Liu YM, Wu GX (2007) Interactions between typhoon and subtropical anticyclone over western Pacific revealed by numerical experiments. Acta Meteor Sinica 65: 329–40

Rodwell MR, Hoskins BJ (2001) Subtropical anticyclones and summer monsoon. J Climate 14: 3192–211

Tao SY, Chen LX (1987) Reveiw in monsoon meteorology. Oxford University Press, pp. 60–92

Sobel AH, Camargo SJ (2005) Influence of western north Pacific tropical cyclones on their large-scale environment. J Atmos Sci 62: 3396–407

Tiedtke M (1989) A comprehensive mass flux scheme for cumulus parameterization in large-scale models. Mon Wea Rev 117: 1779–800

Wu GX, Chou JF, Liu YM, He JH (2002) Dynamics of the formation and variation of subtropical anticyclones. Science Press, Beijing, 314 pp (in Chinese)

Wu GX, Liu H, Zhao YC, Li WP (1996) A nine-layer atmospheric general circulation model and its performance. Adv Atmos Sci 13: 1–18

Wu GX, Liu YM, Liu P (1999) The effect of spatially non-uniform heating on the formation and variation of subtropical high. Part I: Scale analysis. America subtropical high. Acta Meteor Sinica 57: 257–63 (in Chinese)

Wu GX, Liu YM (2000) Thermal adaption, overshooting, dispersion, and subtropical anticyclone Part I: Thermal adaptation and overshooting. Chinese J Atmos Sci 30: 1201–04 (in Chinese)

Wu GX, Liu YM (2003) Summer time quadruplet heating pattern in the subtropics and the associated atmospheric circulation. Geophys Res Lett 30: 1201–04

Yanai M, Esbensen S, Chu JH (1973) Determination of bulk properties of tropical cloud clusters from large-scale heat and moisture budgets. J Atmos Sci 30: 611–27

Yao XP, Wu GX, Liu YM, Liu HZ (2007) Case study on the impact of the vortex in the easterlies over the tropical upper troposphere on the subtropical anticyclone over western Pacific Ocean. Acta Meteor Sinica 65: 198–207 (in Chinese)